Journal Pre-proof

Enhanced chitin gel with magnetic nanofiller for lysozyme purification

Gabriel Ibrahin Tovar Roberto Fernández de Luis María Isabel Arriortua Federico Javier Wolman Guillermo Javier Copello

PII: S1226-086X(20)30143-X

DOI: https://doi.org/doi:10.1016/j.jiec.2020.03.026

Reference: JIEC 5011

To appear in: *Journal of Industrial and Engineering Chemistry*

Received Date: 11 February 2020

Revised Date: 13 March 2020

Accepted Date: 18 March 2020

Please cite this article as: Gabriel Ibrahin Tovar, Roberto Fernández de Luis, María Isabel Arriortua, Federico Javier Wolman, Guillermo Javier Copello, Enhanced chitin gel with magnetic nanofiller for lysozyme purification, *<![CDATA[Journal of Industrial and Engineering Chemistry]]>* (2020), doi: https://doi.org/10.1016/j.jiec.2020.03.026

- Nanofillers of Fe_3O_4 were embedded in Chitin for lysozyme purification
- The increase of Fe_3O_4 modified the cell parameters and porosity of chitin
- Nanofillers influenced chitin structure enhancing lysozyme purification
- This nanocomposite allows one step purification of Hen Egg White Lysozyme
- A 75% global yield and 99% lysozyme purity was obtained from undiluted egg white

Graphical Abstract

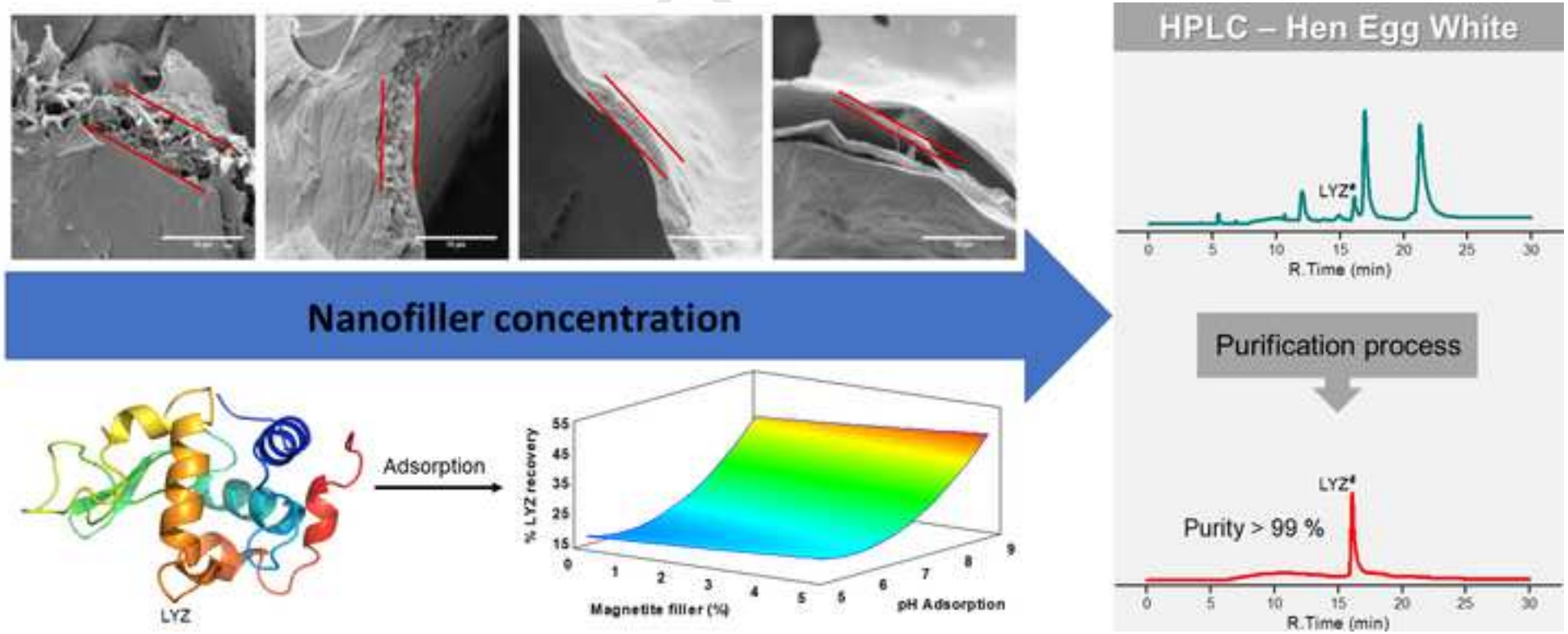

Enhanced chitin gel with magnetic nanofiller for lysozyme purification

Gabriel Ibrahin Tovar[a,b], Roberto Fernández de Luis[c], María Isabel Arriortua[d], Federico Javier Wolman[e,f], Guillermo Javier Copello[a,b,*]

[a] *Universidad de Buenos Aires (UBA), Facultad de Farmacia y Bioquímica, Departamento de Química Analítica y Fisicoquímica, Junín 956, C1113AAD, Buenos Aires, Argentina*
[b] *CONICET – Universidad de Buenos Aires (UBA). Instituto de Química y Metabolismo del Fármaco (IQUIMEFA), Buenos Aires, Argentina*
[c] *BCMaterials (Basque Centre for Materials, Applications and Nanostructures), Bld. Martina Casiano, 3rd. Floor UPV/EHU Science Park Barrio Sarriena, 48940, Leioa, Spain*
[d] *Universidad del País Vasco (UPV/EHU), Departamento de Mineralogía y Petrología, Barrio Sarriena, 48940, Leioa, Spain*
[e] *Universidad de Buenos Aires, Facultad de Farmacia y Bioquímica, Cátedra de Biotecnología, Junín 956, C1113AAD, Buenos Aires, Argentina*
[f] *CONICET – Universidad de Buenos Aires. Instituto de Nanobiotecnología (NANOBIOTEC), Buenos Aires, Argentina*

Abstract

In this study, we have investigated the impact of superparamagnetic magnetite nanoparticle (Fe_3O_4) inclusion on the chitin polysaccharide structure, together with its surface chemistry influence on the adsorption of lysozyme (LYZ). **Magnetic nanoparticles (MNPs) as fillers** not only endow the chitin host structure with their physic and chemical properties but also is a straightforward tool to modify or template its porous structure. Indeed, scanning electron microscopy (SEM) and Brunauer–Emmett–Teller (BET) surface area measurements confirm the template effect of the MNPs on chitin. Their incorporation reduced the thickness of the pore wall and increased the surface area from chitin (34.5 m^2/g) to the Chitin@Fe_3O_4 composites (210.8 m^2/g). MNPs provide the composite system an intrinsic magnetic moment that enables the magnetic recovery of the adsorbent after LYZ uptake. To characterize the magnetic composite's interaction with LYZ, the effect of pH on the absorptive capacities and

*Corresponding author
Email address: gcopello@ffyb.uba.ar (Guillermo Javier Copello)

kinetic parameters was examined. The results indicated that the nanocomposite presents an adsorption capacity of 488 mg/g of lysozyme at pH 9, being able to recover LYZ without diluting or pretreating the hen egg-white, leading to a 75 % global yield and a purity degree >99 % in only one chromatographic step.

Keywords: Chitin, Magnetite, Nanofiller, Protein purification, Lysozyme

1. Introduction

The development of new nanomaterials or immobilization of well-known nanoparticles in biopolymeric matrices has been an intensely growing research field in the last decades. Among all the physic and chemical characteristics that allow to understand the functioning of biocomposites, the biointerface between the biopolymer and the nanoparticle fillers included within them is one of the most important ones to consider [1, 2]. The chemical information encoded at the interface of the bio-polymer and nano-fillers is especially relevant when applying bio-polymer based composites to biomolecules purification. Indeed, the interaction between the adsorbate and the adsorbent plays a crucial role in a biomolecule separation process.

In this sense, metal ions and small molecules interaction with nanobiocomposites have been widely studied. Due to the synergistic effect of both nanoparticles and biopolymer matrix components, the bio-composites have been revealed as highly effective adsorbents for water and air remediation, or as bio-devices for controlled drug delivery applications [3, 4]. Nevertheless, until recently, the scientific community has paid less attention to the large molecules – adsorbent interaction, and hence to the exploration of these bio-composites as adsorption/purification systems for proteins.

Hydrogels based on bio-composites polymers have been intensively studied for protein purification [5]. Compared with the widely studied hydrogels based

on synthetic polymers, such as acrylic acid, acrylamide and poly(ethylene glycol), the hydrogels based on biopolymers, such as alginate [6], carboxymethyl cellulose [7], silk [8], chitosan [9]and chitin derived polymers [10], have recently captured researchers interest due to their biocompatibility, nontoxicity and biodegradability. Moreover, according to their chemical nature, they can perform through different chromatographic interactions.

Chitin has been selected in this work as a biopolymer matrix to immobilize inorganic magnetite bio-compatible fillers. Chitin is a biopolymer with repeating units of N-acetyl glucosamine. It is found in crustacean exoskeletons, fungi, insects, and it is the second biopolymer with the highest availability on earth after cellulose. One of the main advantages of chitin is that is biocompatible, nontoxic and biodegradable, and it is easy to extract by means of low-cost processes [11]. Depending on the processing condition, chitin can be obtained as a polymeric matrix having macro to mesopores within its structure. The interconnected macro-mesoporous structure of the chitin matrix is highly advantageous when considered as a filtering or purification system for proteins [12]. In addition, chitin is an interesting material to be used in the development of absorptive processes because of its chemical and mechanical stability in water and most of the organic solvents.

Besides the affinity of chitin for metal ions and small molecular weight molecules as organic pollutants, the chitin is known to exhibit interesting interactions with proteins. In nature, chitin-protein interactions occur with the family of the glycoside hydrolases, which catalyze the hydrolysis of glycosidic bonds and are key enzymes in carbohydrate metabolism [13]. More concretely, chitin affinity over lysozyme (LYZ) is also known since long time ago. In this regard, the purification of lysozyme in bio-composites is highly relevant for the development of antimicrobial materials on the medical and food industry [14]. One of the reasons is that lysozyme is able to catalyze the hydrolysis of a key component of gram-positive bacterial cell walls.

The advantage of using chitin in the isolation or adsorption of LYZ is that this biopolymer works both as chromatographic support and as ligand [15].

Until recently, most works reported use chitosan, which after its synthesis is acetylated to gain chitin $-COCH_3$ groups for LYZ isolation [16]. Despite chitin processing and handling is more challenging, its high acetylation degree and surface chemistry improve the LYZ−Chitin interaction, adsorption, and migration; which suppose an evident advantage in comparison to chitosan bio-composites.

To further gain LYZ−chitin matrix affinity, as well as to found parallel approaches to template the chitin porous structure, we decided to explore the impact of magnetite nanoparticles fillers inclusion within the chitin porous matrix. The recent advances in the development of polymeric nanocomposites demonstrate that the nanofillers influences the structure of the hosting polymer. Several studies reported that nanoparticles can induce structural changes in a polysaccharide network when a composite is formed [17, 18]. In example, changes in crystallinity and hardness have been reported by introducing MNPs in chitin/cashew gum composites [19]. Other reports demonstrated that MNPs can improve the magnetic and thermal properties of organic polymers [20, 21]. Thus, it would be expected that the use of nanoparticles in a polysaccharide-based nanocomposite could control their structural properties, influencing its performance for LYZ separation. In addition, if magnetic nanoparticles (MNPs) are used as active fillers within the chitin porous matrix, the chromatographic affinity of chitin can be further enhanced with magnetic separation technologies [22].

Magnetite nanoparticles combine the ideal characteristics for this end because of their unique magnetic properties, biocompatibility, and biodegradability. Indeed, they had been approved for human use by the U.S. Food and Drug Administration (FDA) [23]. After the adsorption of LYZ, magnetite containing bio-composites allow easy and rapid isolation of analytes by means of an external magnetic field, which increases the efficiency of solid-phase separation in comparison with raw bio-polymer supports. In this regard, the efficiency of biopolymer-MNPs composites in the purification of LYZ has recently been demonstrated with Hen Egg White Lysozyme (HEWL) samples using MNPs-Poly(N-isopropylacrylamid), where it was shown that both the amount

of nanoparticles and the morphology of the gel affect the adsorption of HEWL [24]. In addition, molecularly imprinted acrylamide/ Fe_3O_4/ SiO_2 MNPs were applied to magnetically separate lysozyme from human urine with great yields [25]. Other studies have employed molecularly imprinted MNPs for the specific recognition of proteins [26, 27].

In this study, the impact of magnetite (Fe_3O_4) as fillers on chitin hydrogels structure and its influence in LYZ separative behavior has been evaluated. In comparison to previously reported biopolymer-MNPs composites; the specific characteristic of the porous chitin matrix make this composites LYZ purification capacity over performing the previously reported systems. Finally, the LYZ purification from undiluted egg white was assessed.

2. Experimental Section

2.1. Materials

Iron sulfate ($FeSO_4 \cdot 7\,H_2O$) and iron chloride ($FeCl_3 \cdot 6\,H_2O$) were obtained from Mallinckrodt (USA). NH_4OH (30 w/v %) was acquired from Biopack (Argentina). Chitin powder (CP, from shrimp shells), LYZ standard and *Micrococcus lysodeikticus* were from Sigma-Aldrich (USA). Calcium chloride dihydrate ($CaCl_2 \cdot 2\,H_2O$ was purchased from Cicarelli (Argentina) and methanol was from Sintorgan (Argentina). Biuret reagent (Proti 2) was kindly donated by Wiener lab (Argentina). The water used was milli-Q quality. All other reagents were analytical grade.

2.2. Synthesis of magnetic nanoparticles

Nanoparticles of Fe_3O_4 were obtained by a modified coprecipitation method [28]. $FeSO_4 \cdot 7\,H_2O$ (250 mmol) and $FeCl_3 \cdot 6\,H_2O$ (500 mmol) (molar ratio 1:2) were added to a flask, and the mixture was mechanically stirred for 30 min at 60 °C. Then, 20 mL ammonium hydroxide (7 %) was dropped into the mixture at a rate of 5 ml/min under vigorous stirring. The resulting black mixture was transferred to a batch sonicator (Elmasonic TI-H-5 Elma, Germany) for 60

min at 35 kHz and 60 °C. The products were collected by magnetic separation and washed with distilled water up to neutral pH. Then MNPs were dried into powder at 60 °C overnight.

The shape of the MNPs was observed using a transmission electron microscope (TEM, Zeiss EM109T). The hydrodynamic particle size (Z-average), size distribution (poly-dispersity index, PDI) and ζ-potential were measured by Dynamic Light Scattering (173°) using a Horiba Nano-SZ 100 analyzer (Horiba, Japan) at 37 °C. The ζ-potential was determined using a technique of Laser Doppler Electrophoresis technique. Average and standard deviation values of Z-average and ζ-potential were obtained from at least 10 determinations for each sample. The MNPs presented a main population of 14 nm with a negative surface charge of -40 mV (Fig. SI-1). The mean hydrodynamic diameter was 137 nm in water, with a distribution ranging from 105 to 315 nm, showing that the MNPs tended to aggregate in liquid media [29].

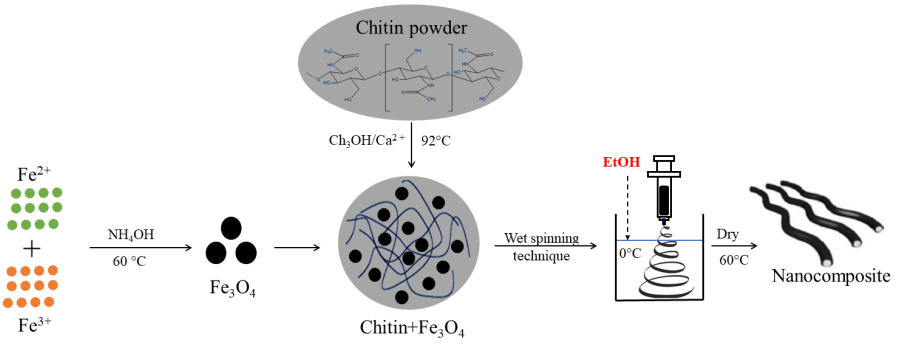

Figure 1: Preparation scheme of Chitin@Fe_3O_4 nanocomposites

2.3. Synthesis of magnetic chitin nanocomposites

The magnetic nanocomposites of Chitin@Fe_3O_4 were prepared by wet-spinning method (Figure 1). $CaCl_2 \cdot 2\,H_2O$ (42.5 g) was suspended in 50 mL of methanol and refluxed for 30 min at 82 °C to a state of near-dissolution. Chitin (1 g) was added to this solution and refluxed for 2 h at 90 °C with stirring [17]. Subsequently, 5, 20, and 50 mg of MNPs were added to a chitin solution to obtain the

nanocomposites, named MC5, MC20, and MC50, respectively. The chitin gel without MNPs was named CHI. The mixtures were spun in cold methanol until gelled and washed several times with distilled water. Finally, the gel strand was dried in a stove at 60 °C until constant weight, ground, and sieved between 250-500 μm.

2.4. Structural characterization of nanocomposites

The morphology of the nanocomposites was examined using scanning electron microscopy (SEM, FEI, Quanta 250 FEG).The fillers dispersion in the nanopomposite was observed by energy dispersive X-ray spectroscopy mapping (EDX, Phillips). To obtain the surface areas, CO_2 adsorption isotherms at 77 K were measured by multipoint Brunauer−Emmett−Teller (BET) apparatus (Quantachrome Autosorb−iQ−MP analyzer, USA). All samples were dried under vacuum at 80 °C for 6 h to eliminate solvent guest materials prior to measurements. Samples were hydrated in water for 24 h and lyophilized as pretreatment for SEM and BET. The FTIR spectra were registered in the range 500-4000 cm^{-1} with 4 cm^{-1} spectral resolution by performing 64 scans with an ATR-FTIR Thermo Nicolet iS50 spectrometer (Thermo Scientific, MA, USA). The X-ray diffraction powder (XRD) patterns were obtained by a Panalytical X'pert PRO diffractometer (Cu Kα 1,2 radiation), 2θ range = 5-70°, step size = 0.015°, exposure time = 10 s per step at room temperature. The patterns were fitted by Le Bail method [30], using Fullprof software [31]. The magnetic properties were measured at room temperature using a vibrating sample magnetometer (VSM; LakeShore Model 7410, USA) with a maximum magnetic field of 10 kG. Thermogravimetric analysis was performed under synthetic air with a DSC-TGA instrument (Netzsch STA 449F3, Selb, Germany). The samples (7 mg) were heated at 10 °C/min in the temperature range 30 − 700 °C.

2.5. Lysozyme adsorption studies

Adsorption experiments were carried out in batch systems with controlled temperature (25 °C for 16 h) and mechanical agitation. Response surface

methodology (RSM) according to a Box-Behnken factorial design was applied in order to evaluate the optimum condition for adsorption and elution efficiency of LYZ. Factorial design of 2^4 was established to obtain theoretical models that define the most favorable conditions for LYZ adsorption. The independent variables selected were: adsorption medium pH (pH: 5, 7, 8 and 9), and MNPs concentration on nanocomposites (Fe: 0, 0.5, 2 and 5 mg/g); whereas the dependent variables were the Recovery Rate (Y1), Adsorption (Y2), and Elution (Y3). The 16 experiments established by the factorial design were made by triplicate according to multilevel factorial design, obtained a total of 48 experiments that were carried out in 1 mL LYZ solution (3 mg/ml) and 10 mg of nanocomposite, with pH and MNPs according to the RSM. The correlation between independent variables and the dependent variable was expressed on the terms of a regression adjusted from the experimental data. The regression coefficient parameters of the polynomials equations were estimated using the Statgraphics software.

The interaction times, and adsorption isotherms was determined for LYZ by quantification before and after incubation with the matrices tested. To this end, the pH of LYZ solutions was adjusted using acetate citrate (20 mM, pH 5.2), phosphate buffer (20 mM, pH 7 and 8), or carbonate buffer (20 mM, pH 9.4). For the isotherm analysis, a weighted mass of gel nanocomposite (corresponding to 10 mg dry weight) was added to an aqueous LYZ solution (1 mL) ranging from 0.0313 to 15 mg/ml. LYZ concentration in supernatants at equilibrium was then measured spectrophotometrically at 280 nm using a Shimadzu UV-1800 spectrometer (Shimadzu Inc., Kyoto, Japan). The parameters of the kinetic and isotherm models were estimated using a nonlinear optimization (detailed equations is given in Supplementary Information).

2.6. Lysozyme purification from hen egg white

Purification processes were studied using 100, 50, or 25 mg of an equilibrated matrix in the adsorption buffer (20 mM carbonate, pH 9.0) incubated with 1 mL egg white for 4 h at room temperature, with gentle agitation. Adsorbed lysozyme was calculated as the difference between the amount of lysozyme in the

egg white and that in the supernatant after adsorption. After three washing steps with adsorption buffer, the enzyme was eluted with 1 mL 0.1 M acetic acid. After regeneration with 0.05 M of NaOH, the matrix was re-utilized for three new purification cycles. Total protein content was calculated by the Biuret method.

2.7. Analytical assays

The enzymatic activity of LYZ was measured by its lytic action on *Micrococcus lysodeikticus*. To this end, 25 μL of the sample were added to 975 μL of a *M. lysodeikticus* suspension (0.5 mg/mL) in 20 mM potassium phosphate buffer (pH 7.0). Absorbance at 450 nm was measured every 10 s for 2 min, defining one unit of LYZ activity as a decrease in 0.001 absorbance units per minute. The process isolation and purity degree of HEWL were tested at 280 nm by RP-HPLC chromatography (HPLC Shimadzu LC-20AT System, Kyoto, Japan) with a C18 ACE HPLC column (4.6 mm x 25 cm, 300 Å, 5 μm, Advanced Chromatography Technologies, Aberdeen, Scotland) using conditions report previously [9]. Mobile phase A was 0.065% trifluoroacetic acid (TFA) in water, and mobile phase B was 0.050% TFA in acetonitrile, at a flow rate of 1 mL/min. The samples collected were previously filtered with nylon membranes of 0.22 μm (GVS life science, USA). A 20 μL injection volume was used to analyze all samples from the purification process. The chromatogram gradient was performed as 0-5 min from 0% to 25% B, 6-25 min from 25% to 80% B, and 25-30 min holding 100%. The peak areas were determined to calculate the purity degree (%).

3. Results and Discussion

3.1. Structural characterization of the nanocomposites

The diffusion of a protein within an adsorbent is associated to the interconnected porous structure of the matrix. In a first attempt, this was studied by means of scanning electron microscopy (SEM) images and EDX elemental

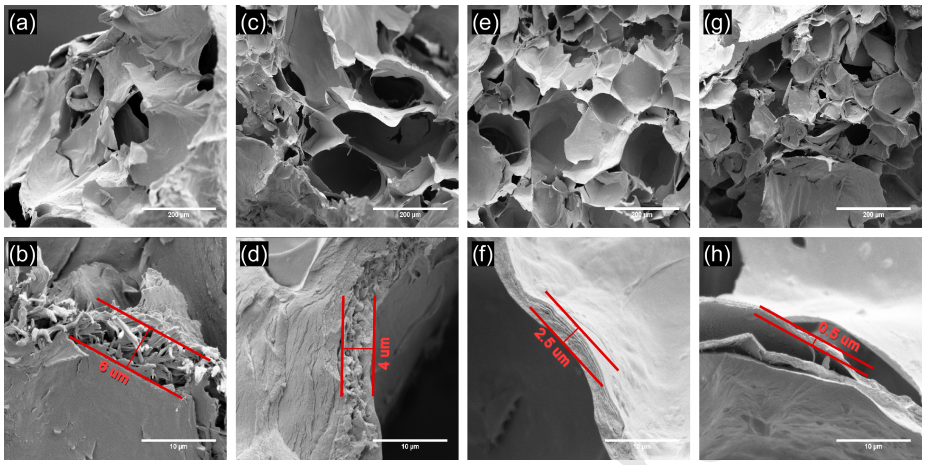

Figure 2: SEM micrographs. (A,B) CHI 500x and 10,000x; (C,D) MC5 - 500x and 10.000x; (E,F) MC20 - 500x and 10.000x; (G,H) MC50 - 500x and 10.000x.

mapping and showed in the Figure 2 and Figure SI-2. The chitin magnetite composites had a well-developed pore structure, with a homogeneous dispersion of Fe_3O_4 MNPs within the chitin matrix. Chitin structure can be described as macro-pores defined by chitin walls; which also have an internal stranded mesostructured morphology. Magnetite filler incorporation to chitin influenced both the macro-pore size together with the thickness and internal mesostructure of the chitin walls.

SEM images showed macropore sizes ranging between 50 and 150 μm for chitin. The macropore size decreased with increasing MNPs content in the nanocomposite. In parallel, the wall diameter was reduced considerably from 6 μm in CHI to 4, 2.5 and 0.5 μm for MC5, MC20 and MC50, respectively. With the increase in MNPs content, these strands became compressed, indicating that the MNPs induced a conformational change in the chitin polymeric arrangement. BET analysis supports the porous structure change induced by the magnetic nanoparticles, since the surface area increase from 34.5 m^2/g for CHI and 210.8 m^2/g for MC50. The conformational change in chitin structure that led to the pore wall compression in the nanocomposite probably led to a higher surface area.

The apparent density of the nanocomposites was tested by mass and geometric volume, the obtained values are shown in Figure SI-3. The apparent density increased proportionally with increasing nanofiller content up to MC20 and followed a non-lineal response for MC50. Due to the relation between apparent density and the nanofiller loading, in order not to surpass the percolation threshold of the hydrogel, MC50 was chosen as the higher concentration to study [32]. The nanofillers incorporated would be determinant of the extent of physical connection between the polymers chains. Such a result was positively correlated with the variations in the pore morphology observed by SEM.

The internal structure of the matrix plays significant role in the performance of an adsorbent. The pore surface is the physical place where the ligand-protein interaction occurs. The 3D structure defines the internal surface area and porosity. Moreover, when the target molecule is a protein with a diameter of several nanometers, macroporous (>50 nm) or gigaporous matrices would be desired in order to let the adsorbate reach every adsorption site available without the need for extremely long equilibrium times or elevated pressures.

3.2. Spectroscopic and magnetic characterization

The ATR-FTIR spectra of MNPs and the nanocomposites are discussed in the Supplementary section, Figure SI-4. For the nanocomposites, it was not possible to detect any new vibrational modes, displacements, or disappearance of any pre-existing bands in comparison to the FTIR spectra of each individual chitin and magnetite components. This points out the lack of strong chemical bonds between chitin and MNPs. Thus, the changes observed in chitin porous structure were mainly due to the influence of MNPs in chitin structuring during the gelling stage. At the crystal structural level, Figure 3 shows the XRD patterns of the MNPs, MC50, and chitin. As expected, the XRD patterns of MNPs present diffraction maxima at 30.42 (220), 35.80 (311), 43.51 (400), 53.89 (422), 57.43 (511), and 63.07 (440) in $2\vartheta(^{o})$, fully consistent with the calculated pattern obtained from Fe_3O_4 magnetite structural model [33]. The Scherrer's equation (1) was used to calculate an average crystalline size of crystallite size

of 12.6 ± 0.5 nm; which is close to the value obtained from the TEM image analysis mentioned before

$$D = \frac{K\lambda}{\beta \cos\theta} \tag{1}$$

where = D: average crystallite size; K: Scherrer constant, λ: the wavelength of XRD; β: peak width; θ: scattering angle

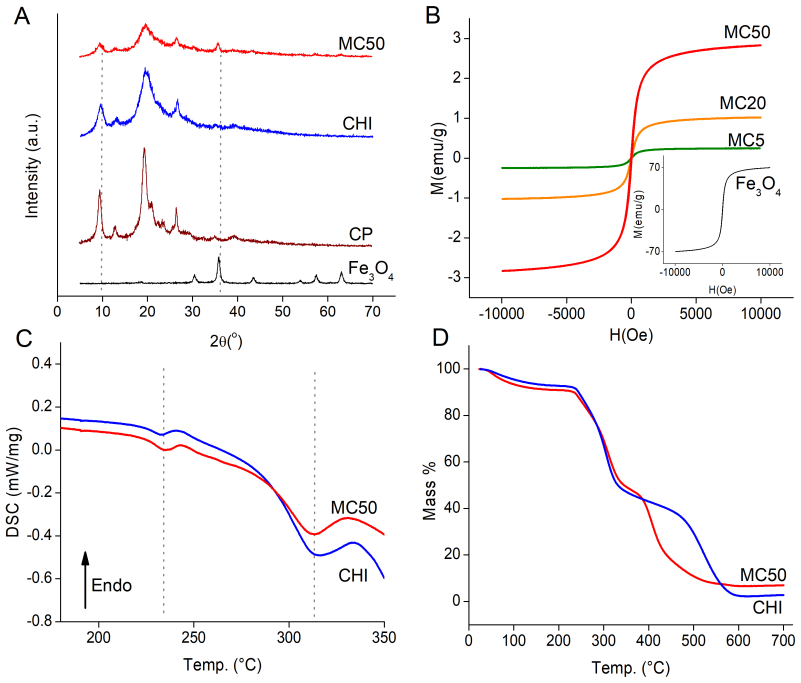

Figure 3: Structural characterization of material. (A) X-ray diffraction (XRD); (B) Vibrating-sample magnetometer (VSM); (C), DSC; (D), TGA. Data for CP (brown), CHI (blue), Fe_3O_4 (black), MC5 (green), MC20 (yellow) and MC50 (red).

For CHI and Chitin@Fe_3O_4 composites, an initial visual inspection of the X-ray diffraction patterns clearly indicates the presence of α-Chitin phase. Afterwards, the diffraction patterns were initially adjusted with a Le-Bail profile matching, starting from the cell parameters and orthorhombic symmetry reported for the α-Chitin by Tanner [34]. Cell parameters and profile variables were refined until convergence. For the Chitin@Fe_3O_4 composite, a two-phase

Le-Bail refinement was carried out including the magnetite cell parameters and symmetry within the model. Final fits for the three samples (Figure SI-5) confirm the presence of cubic Magnetite nanoparticles within the Chitin polymer matrix.

In addition to a peak broadening of the CHI and MC50 composite in comparison with untreated chitin powder (CP), all the Le-Bail analyses show specific (hkl) broadening that induce a meaningful mismatch between the experimental and the modeled profiles. This evidence points toward anisotropic crystallographic stress of specific structural units, more probably ascribed to the degree of order of the chitin chains along with different crystallographic directions. Despite this experimental mismatch, the final fittings have enough accuracy to determine the cell parameters and peak positions for the α-Chitin and magnetite phases in the composites (Table 1). Indeed, a cell parameter increase from the CHI to CP and Chitin@Fe_3O_4 samples were observed. This means that the processing of CP into gels (CHI), or the incorporation of Fe_3O_4 nanoparticles within the CHI, not only altered the macroscopic structure of chitin polymer but also induces a slight reorganization of the polysaccharide chains. In fact, the increase in the b parameter, being more affected by the process, suggests that the main structural re-arrangements occurred along the polysaccharide chains stacking along the [010] crystallographic direction.

The observed changes in the lattice parameters would be a response of the interaction forces arose from the interfacial contact between MNPs and chitin. The polymer chains at the proximity of the nanofillers can be stretched, thus leading to a decrease of their conformational entropy. The presence of a rigid interface could drive the segregation of lower molecular weight chains during the hydrogel formation upon the wet-spinning process [35]. These phenomena are due to modification of the polymer segmental mobility and that of purely geometric factors [36]

A comparison of the crystalline index (CI %) was performed according to the following equation [37]: CI_{110}=[(I_{110}-I_{am})/I_{110}]x100, where I_{110} is the maximum intensity at approximately 2θ 19°. The intensity of the [012] reflection

associated with the amorphous diffraction part of the polymer, I_{am}, was obtained at approximately 12°. Final values for the crystallinity index and cell parameters are summarized in Table 1.

Table 1: Crystallinity index and cell parameters

Sample	CP	CHI	MC50
CI_{110}	80	72	69
a (Å)	4.69 (1)	4.64 (15)	4.74 (7)
b (Å)	18.76 (5)	18.80 (2)	19.10 (4)
c (Å)	10.20 (3)	10.03 (12)	10.27 (2)

The magnetic properties of the materials were analyzed by means of VSM. Figure 3 exhibits the hysteresis loops of the MNPs and the nanocomposites, fitted with the Langevin model. The saturation magnetization, Ms, remanent magnetization, Mr, and the coercive field, Hc, are shown in Table 2. As dispersing agents can influence the magnetic properties of nanocomposites [38], the saturation magnetization of the Chitin@Fe_3O_4 was evaluated. The MNPs showed 283 a magnetic saturation of 70 emu/g and an S-type hysteresis loop. As can be seen, Mr values increased from MC5 to MC50, proportionally to the quantity of MNPs added to the nanocomposites. This implies that the synthesis process or the chitin matrix did not affect the magnetic properties of the particles. The coercive force Hc decreases tending to zero due to the superparamagnetic relaxation effects typical for nanoparticles with a diameter approximate to 10 nm [39]. At room temperature, the remanence-to-saturation ratio, $R = Mr/Ms$, for all samples was smaller than 0.5, as expected for non-interacting randomly oriented particles with uniaxial symmetry. Moreover, these R values revealed the existence of weak interparticle interactions of antiferromagnetic nature [39].

As shown in Figure 3C-D, the thermal analyses demonstrate that the inclusion of MNPs in the polymer network influence chitin thermal transitions. The exothermic peak observed in CHI at 228 °C increased its characteristic temperature to 234 °C in MC50. This peak has been assigned to the loss of

Table 2: Magnetic properties of Fe_3O_4 and nanocomposites.

Sample	Ms (emu/g)	Mr (emu/g)	Hc (Oe)	Mr/Ms
Fe_3O_4	70.0	1.49	14.58	0.02
MC50	2.85	0.02	5.97	0.01
MC20	1.03	0.01	5.58	0.01
MC5	0.26	0.02	5.72	0.07

hydroxyl groups in chitin [40], and this temperature increase could be related to the tightening of the polymer network and the subsequent increase in the chain interaction, an effect that could also explain the porous and crystallographic changes observed by SEM images and described in the XRD results. The exothermic acetamide group decarboxylation observed for CHI at 316 °C, was increased by the presence of the MNPs in MC50 to 316 °C. The TG analysis (Figure 3) showed that the previously mentioned DSC transitions were accompanied by the correspondent mass loss at a similar temperature range. For higher temperatures, further decomposition of the nanocomposite can be observed as a mass loss. It is worth to mention that the introduction of MNPs decreased this decomposition temperature, which appeared at 500 °C for CHI and at 390 °C for MC50. This decrease could have been originated in a catalytic effect induced by the presence of Fe_3O_4 [41]. The differences in the residual mass for CHI and MC50 were 5.4% which accounted for the amount of Fe_3O_4 present in the MC50 nanocomposite (5 % w/w Fe_3O_4/chitin). The above stated indicates that during the synthesis of the nanocomposite and its further processing there was no loss of MNPs, supporting the XRD and VSM results.

Taking into account the described results, it is proposed that the chemical interaction between chitin and the MNPs is negligible and the main effect of the presence of the filler took place at the gelling stage. During gelling, at the wet-spinning process, the polysaccharide chains were induced to interact with themselves by the dilution of $CaCl_2$. At this point, the presence of the

filler would hinder the interaction between chitin chains leading to a different structural conformations. It can be concluded that the difference between the chitin hydrogel and the Chitin@Fe_3O_4 composites is associated to the structuring of the polysaccharide chains that impact in the pore structure and its surface, two critical parameters that could lead to an enhanced LYZ-chitin interaction during the adsorption-elution purification process.

3.3. Effect of filler content in LYZ adsorption study.

The steps of Adsorption, Elution and the global Recovery Rate (RR) of LYZ by the materials were analyzed in order to understand the influence of the nanofiller in LYZ purification. With this aim, an experimental design was performed, as shown in Figure 4. A regression analysis was carried out to fit mathematical models to the experimental data, aiming at an optimal region for the responses studied. The predicted model can be described by equations (2), (3) and (4) in terms of coded values:

$$RR = K_{RR} + 0.146 * Fe - 31.5 * pH + 0.09 * Fe * pH \quad (2)$$

$$Ads = K_{Ads} + 2.1 * Fe + 31.1 * pH - 0.435 * Fe * pH \quad (3)$$

$$Elution = K_{Elut} + 5.2 * Fe + 0.61 * pH - 0.86 * Fe * pH \quad (4)$$

where =Ads: Adsorption ;K_{RR}: 108 ; K_{Ads}: 25.7; K_{Elut}: 38.5; pH: pH used in the adsorption process; Fe: mass of iron oxide nanoparticles per gram of biopolymer (mg/g).

As can be seen in Figure 4 A-C, both the pH and the amount of iron in the nanocomposite have a influence in chitin-LYZ interaction and proved to be significantly different between treatments (p <0.01, ANOVA). It was expected

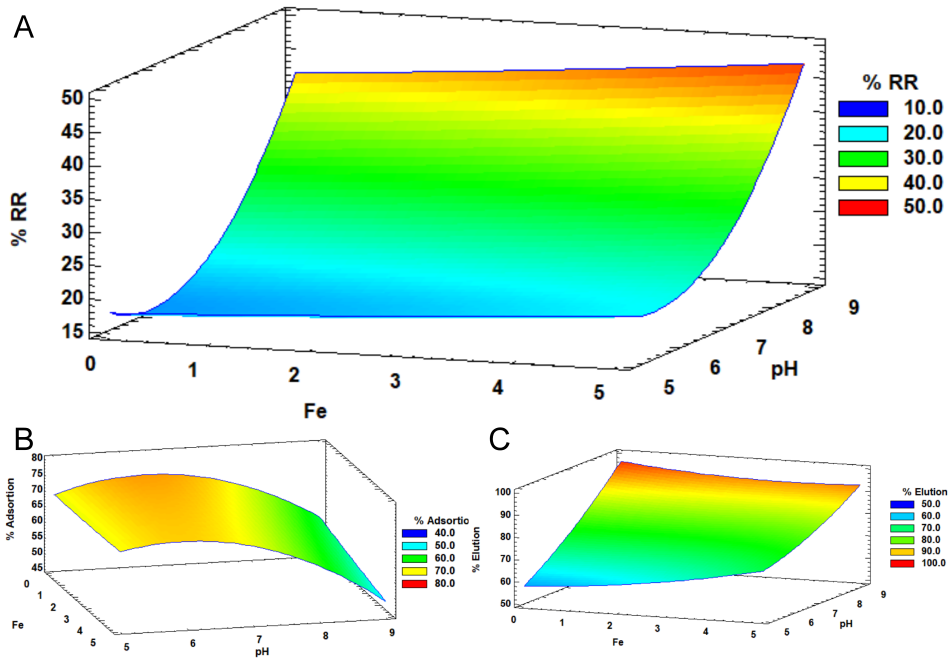

Figure 4: Estimated response surface for LYZ. (A) Recovery Rate (RR); (B) Adsorption; (C) Elution.

that the pH present a predominant effect in in the adsorption stage of the chitin-lysozyme interaction and, therefore, on the Recovery Rate. Although, the effect of the iron content was less evident than the pH effect, it showed to affect the chitin-LYZ interaction in this step and, therefore, need to take into account in the optimization of a purification process. The fitted equations for adsorption and elution showed that the effect of the increase in the iron content in the nanocomposite was higher for the elution step than for the adsorption step in comparison to the effect of pH. This could be expected but it is not always straight forward since the adsorption pH may alter the structure of the protein, i.e. by denaturing, and affect the desorption stage. The combined effect of a higher adsorption at a high pH and a high desorption with the increase of the iron content in the nanocomposite could be the reason of the higher RR observed at the higher (pH 9) and for the higher iron content (MC50). This

also agrees with the efficiency of elution capacity of MC50 with respect to the other nanocomposites and MNPs, and adsorption capacity of LYZ at each pH (Figure SI-6). In order to understand fully lysozyme adsorption and elution process in Chitin@Fe_3O_4 composites, MC50 was selected to develop the full LYZ absorption kinetic, equilibrium studies and its purification from egg white.

3.4. LYZ absorption kinetic, equilibrium studies and purification from egg white

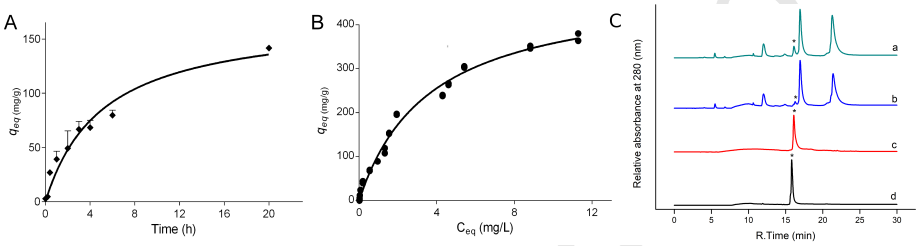

Figure 5: LYZ adsorption studies. (A) Kinetic assay; (B) Equilibrium assay; (C) RP-HPLC of the purification process. Egg white (a), egg white after adsorption (b), eluted sample (c), LYZ commercial 1 mg/mL (d). (*) LYZ

The advantages of the development of a magnetic nanocomposite for the purification of LYZ were studied from the operative point of view. Lysozyme adsorption kinetic experiments were carried out to assess the adsorption rate of lysozyme onto MC50, as shown in Figure 5 A. The results showed that the adsorption process of lysozyme achieved the equilibrium condition beyond 4 h. In order to describe the behavior of the lysozyme adsorption, pseudo-first-order (RMSE = 11.66) and pseudo-second-order (RMSE = 10.07) kinetic models were used to elucidate the lysozyme adsorption process. The lowest RMSE was obtained for the pseudo-second-order kinetic model, indicating that this model was more appropriate to describe the lysozyme adsorption process. Figure 5 B shows the equilibrium assay with a good fit (RMSE = 13.60) to the Langmuir model and a maximum calculated capacity (qm) of 488 ± 17 (mg/g). The calculated Kd value was 0.27 ± 0.02 mg/mL. Freundlich model (RMSE = 18.45) was also evaluated. The Chitin@Fe_3O_4 nanocomposite was applied to the direct extraction of HEWL. To optimize the purification process, we performed a kinetic

assay and compared the absorption capacity of diluted and undiluted egg white (Figure SI-7). The preconditioning of the sample did not present significant differences (p <0.05, Wilcoxon test), and after 4 h of incubation in both systems (diluted and non-diluted egg white), the equilibrium condition was reached.

Figure 5C shows the chromatograms of egg white solutions before and after the batch process. There were four major proteins in the egg white solution. After the extraction step, three of them remained in the supernatant. In the eluted solution only lysozyme was detected. Results show that Chitin@Fe_3O_4 selectively adsorbed the lysozyme from egg white, allowing the extraction and purification of lysozyme with >99 % purity, calculated from the chromatogram peak areas. This demonstrated the biospecificity of this matrix for LYZ with the added advantage of directly using undiluted egg white as the starting material. In addition, the nanocomposite reusability was tested. After three consecutive purification processes, yield and purity degree parameters remained almost constant (performance decrease <5 %). Also, biofouling would be negligible or, if present, would not affect the performance of the material after three cycles of use. It is worth mentioning that, the complex biological nature of the egg white, mainly due to its high viscosity, makes it a difficult sample to process by chromatographic media [42]. In fact, most of the works reported required diluting the egg white before performing the purification [9, 43, 44], which precluded its subsequent commercialization. However, in this work the purification of lysozyme was achieved in one step directly from undiluted egg white. Moreover, the recovery of the chitin matrix from the adsorption media was performed by using a simple magnet.

Table 3 shows the parameters obtained for the HEWL purification process. No significant differences were observed in LYZ adsorption with the three ratios (volume sample/matrix amount) tested. In all cases, about 90 % of the LYZ was bound to the matrix. The capacity of LYZ recovery, dependent on the ratio of the matrix used, was 99, 78 and 75 % for 100, 50 and 25 mg of matrix used in the process. Diffusive effects were probably responsible for this phenomenon. The global yields were between 75 and 60 %. Diffusive mechanisms could have

Table 3: Purification Process Parameters

M (mg)	Adsorbed (%)	Eluted (%)	RR (%)	Y (%)
100	87±1.4	86±0.2	99	75
50	88±0.3	69±0.2	78	60
25	93±0.8	70±2.1	75	65

RR: Rate recovery. Y: Yields. M: Amount Matrix

affected the recovery and yields of the process. When a high amount of matrix is available, the enzyme is preferably adsorbed onto the external pores of the material. By contrast, when a low amount of matrix is used, the saturation of the adsorption sites at the external pores allows the enzyme to penetrate into the internal pores. Therefore, the porosity, the connectivity network of the pores, the tortuosity of the material, as well as the size of the protein affected the adsorption/desorption steps and may hinder the overall yield of the process [45, 46].

Table 4: Comparison of the maximum adsorption capacities of LYZ on chitin derived adsorbents

Material	Method synthesis	Time (h)	pH	Egg White	Maximum adsorption capacity	HEWL Yield %	Ref.
Chitin-F3O4	Nanofiller of Fe3O4 on pristine chitin. Hydrogel obtained for Wet-spinning	2	9	Undiluted	488 mg/g	75.00	This Work
Chitin-F3O4	Fe3O4/chitosan for Core shell and postsythesis acetylation	72	6.5	ND	154 mg/g	ND	[16]
Chitin-F3O4	Fe3O4/chitosan for Core shell and postsythesis acetylation	0.5	7	Diluted 1/4	2.5 mg/ml	ND	[47]
Chitin-F3O4	Chitin for acid hydrolyzed/ magnetite monolithic cryogel by embedding	0.25	7	Diluted 1/4	3 mg/ml	ND	[48]
O-carboxymethyl chitosan (O-CMCS)-Cu2+	Cu2+-linked O-CMCS Schiff base granules into cryogels	ND	8	Diluted 1/4	103 mg/g	88.2	[49]
chitin–silica	Polymerisation of silica on pristine chitin.	10	8	Diluted 1/4	117 mg/g	87.00	[15]
Chitosan-Sulfanilic Acid	coupling of sulfanilic acid on chitosan mini-spheres	4	7	Diluted 1/4	50 mg/g	81.90	[9]
carboxymethyl chitosan/ Fe3O4 /polyethylene glycol	Coating of Fe3O4	1	9	Diluted 1/2	256.4 mg/g	85.2	[44]

ND: No date

The results revealed that the nanocomposite Chitin@Fe_3O_4 here presented, could be a very promising adsorbent material to be used for large-scale separation

of lysozyme from egg white. Table 4 shows a comparison with other functionalized chitin based adsorbents which were aimed to the adsorption of lysozyme. The maximum equilibrium adsorption capacity presented in this work was considerably higher than some other materials published before and direct HEWL purification was performed with no need of dilution .

4. Conclusions

The impact of Fe_3O_4 MNPs incorporation in the chitin and crystallographic structure together with their influence on the LYZ purification were studied. The Chitin@Fe_3O_4 composite synthesis was simple and scalable and did not alter the structure and magnetic properties of MNPs. In addition, the introduction of MNPs on chitin gels has a template effect of the macro-porous structure together with the internal mesoporosity and arrangement of chitin walls that is reflected in a tenfold increase of the surface area. The presence of the MNPs in the composite material enhanced the performance of the LYZ purification process, mainly leaded by an improvement of the elution step. MC50 composite exhibits a maximum LYZ adsorption capacity that probed to be higher than that of other published materials. In addition, the nanocomposite was successfully used to separate LYZ directly from undiluted egg white in a simple, specific, high yield and low-cost process based on magnetic separation.

5. Acknowledgement

G.I.T. is grateful for his doctoral fellowship granted by Consejo Nacional de Investigaciones Científicas y Técnicas (CONICET). INTI Mecánica and M. Pianetti are also acknowledged for their assistance in SEM analysis. CNEA-Balseiro Institute and A. Butera for their assistance in VSM analysis. This work was supported by the Universidad de Buenos Aires [UBACYT-20020170100125-BA; UBACYT-20020170100023-BA]; and the Agencia Nacional de Promoción Científica y Tecnológica [PICT-0714, 2015; PICT-0845, 2017]. The authors acknowledge the XRD, BET and thermogravimetric measurements performed

under the frame of Ministerio de Economía y Competitividad [MAT2016-76739-R (AEI/FEDER, EU)].

References

[1] S. Kheiri, X. Liu, M. Thompson, Nanoparticles at biointerfaces: Antibacterial activity and nanotoxicology, Colloids and Surfaces B: Biointerfaces 184 (2019) 110550. doi:https://doi.org/10.1016/j.colsurfb.2019.110550.

[2] A. Tofanello, J. N. Araujo, I. L. Nantes-Cardoso, F. F. Ferreira, J. A. Souza, D.-W. Lim, H. Kitagawa, W. Garcia, Ultrafast fabrication of thermally stable protein-coated silver iodide nanoparticles for solid-state superionic conductors, Colloids and Surfaces B: Biointerfaces 176 (2019) 47 – 54. doi:https://doi.org/10.1016/j.colsurfb.2018.12.059.

[3] M. L. P. Ramos, J. A. González, S. G. Albornoz, C. J. Pérez, M. E. Villanueva, S. A. Giorgieri, G. J. Copello, Chitin hydrogel reinforced with TiO_2 nanoparticles as an arsenic sorbent, Chemical Engineering Journal 285 (2016) 581–587. doi:https://doi.org/10.1016/j.cej.2015.10.035.

[4] A. Pourjavadi, M. Kohestanian, M. Shirzad, Synthesis and characterization of magnetic hybrid nanomaterials via raft polymerization: A ph sensitive drug delivery system, Colloids and Surfaces B: Biointerfaces 174 (2019) 153 – 160. doi:https://doi.org/10.1016/j.colsurfb.2018.11.006.

[5] Y.-M. Fang, D.-Q. Lin, S.-J. Yao, Review on biomimetic affinity chromatography with short peptide ligands and its application to protein purification, Journal of Chromatography A 1571 (2018) 1 – 15. doi:https://doi.org/10.1016/j.chroma.2018.07.082.

[6] J. Li, J. Ma, S. Chen, Y. Huang, J. He, Adsorption of lysozyme by alginate/graphene oxide composite beads with enhanced stability and me-

chanical property, Materials Science and Engineering: C 89 (2018) 25 – 32. doi:https://doi.org/10.1016/j.msec.2018.03.023.

[7] F. Marques, G. Silva, M. Thrash, A. Dias-Cabral, Calorimetric approach to understand ph and salt influence on the adsorption mechanism of lysozyme to a traditional cation exchanger, Colloids and Surfaces B: Biointerfaces 185 (2020) 110589. doi:https://doi.org/10.1016/j.colsurfb.2019.110589.

[8] S. Yi, F. Dai, Y. Ma, T. Yan, Y. Si, G. Sun, Ultrafine silk-derived nanofibrous membranes exhibiting effective lysozyme adsorption, ACS Sustainable Chemistry & Engineering 5 (10) (2017) 8777–8784. doi:https://doi.org/10.1021/acssuschemeng.7b01580.

[9] D. B. Hirsch, M. F. Baieli, N. Urtasun, J. M. Lázaro-Martínez, R. J. Glisoni, M. V. Miranda, O. Cascone, F. J. Wolman, Sulfanilic acid-modified chitosan mini-spheres and their application for lysozyme purification from egg white, Biotechnology progress 34 (2) (2018) 387–396. doi:https://doi.org/10.1002/btpr.2588.

[10] Ö. Acet, T. Baran, D. Erdönmez, N. H. Aksoy, İ. Alacabey, A. Menteş, M. Odabaşi, O-carboxymethyl chitosan schiff base complexes as affinity ligands for immobilized metal-ion affinity chromatography of lysozyme, Journal of Chromatography A 1550 (2018) 21–27. doi:https://doi.org/10.1016/j.chroma.2018.03.022.

[11] H. E. Knidri, R. Belaabed, A. Addaou, A. Laajeb, A. Lahsini, Extraction, chemical modification and characterization of chitin and chitosan, International Journal of Biological Macromolecules 120 (2018) 1181 – 1189. doi:https://doi.org/10.1016/j.ijbiomac.2018.08.139.

[12] E. Bulut, I. Sargin, O. Arslan, M. Odabasi, B. Akyuz, M. Kaya, In situ chitin isolation from body parts of a centipede and lysozyme adsorption studies, Materials Science and Engineering: C 70 (2017) 552–563. doi:https://doi.org/10.1016/j.msec.2016.08.048.

[13] A. G. Hamre, E. E. Frøberg, V. G. Eijsink, M. Sørlie, Thermodynamics of tunnel formation upon substrate binding in a processive glycoside hydrolase, Archives of biochemistry and biophysics 620 (2017) 35–42. doi:https://doi.org/10.1016/j.abb.2017.03.011.

[14] T. Wu, Q. Jiang, D. Wu, Y. Hu, S. Chen, T. Ding, X. Ye, D. Liu, J. Chen, What is new in lysozyme research and its application in food industry? a review, Food Chemistry 274 (2019) 698–709. doi:https://doi.org/10.1016/j.foodchem.2018.09.017.

[15] F. J. Wolman, G. J. Copello, A. M. Mebert, A. M. Targovnik, M. V. Miranda, A. A. N. Del Cañizo, L. E. Díaz, O. Cascone, Egg white lysozyme purification with a chitin–silica-based affinity chromatographic matrix, European Food Research and Technology 231 (2) (2010) 181–188. doi:https://doi.org/10.1007/s00217-010-1263-1.

[16] N. A. Samoilova, M. A. Krayukhina, Synthesis of magnetic chitin–adsorbent for specific proteins, Carbohydrate Polymers 216 (2019) 107 – 112. doi:https://doi.org/10.1016/j.carbpol.2019.03.048.

[17] J. A. González, M. E. Villanueva, M. L. P. Ramos, C. J. Pérez, L. L. Piehl, G. J. Copello, Chitin based hybrid composites reinforced with graphene derivatives: a nanoscale study, RSC Advances 5 (78) (2015) 63813–63820. doi:https://doi.org/10.1039/C5RA13563J.

[18] J. A. González, J. G. Bafico, M. E. Villanueva, S. A. Giorgieri, G. J. Copello, Continuous flow adsorption of ciprofloxacin by using a nanostructured chitin/graphene oxide hybrid material, Carbohydrate Polymers 188 (2018) 213 – 220. doi:https://doi.org/10.1016/j.carbpol.2018.02.021.

[19] M. Ramesan, P. Privya, P. Jayakrishnan, G. Kalaprasad, B. Bahuleyan, M. Al-Maghrabi, Influence of magnetite nanoparticles on electrical, magnetic and thermal properties of chitin/cashew gum biopolymer nanocom-

posites, Polymer Composites 39 (S1) (2018) E540–E549. doi:https://doi.org/10.1002/pc.24688.

[20] P. Jayakrishnan, M. Ramesan, Synthesis, structural, magnetoelectric and thermal properties of poly (anthranilic acid)/magnetite nanocomposites, Polymer Bulletin 74 (8) (2017) 3179–3198. doi:https://doi.org/10.1007/s00289-016-1883-0.

[21] P. Jayakrishnan, M. Ramesan, Temperature dependence of the electrical conductivity of poly(anthranilic acid)/magnetite nanocomposites and the applicability of different conductivity models, Polymer Composites 39 (8) (2018) 2791–2800. doi:https://doi.org/10.1002/pc.24271.

[22] M. Wierucka, M. Biziuk, Application of magnetic nanoparticles for magnetic solid-phase extraction in preparing biological, environmental and food samples, TrAC Trends in Analytical Chemistry 59 (2014) 50–58. doi:https://doi.org/10.1016/j.trac.2014.04.007.

[23] D. Bobo, K. J. Robinson, J. Islam, K. J. Thurecht, S. R. Corrie, Nanoparticle-based medicines: A review of fda-approved materials and clinical trials to date, Pharmaceutical Research 33 (10) (2016) 2373–2387. doi:10.1007/s11095-016-1958-5.

[24] E. Alveroglu, N. İlker, M. T. Shah, K. Rajar, A. T. Gokceoren, K. Koc, Effects of gel morphology on the lysozyme adsorption and desorption kinetics of temperature sensitive magnetic gel composites, Colloids and Surfaces B: Biointerfaces 181 (2019) 981 – 988. doi:https://doi.org/10.1016/j.colsurfb.2019.05.062.

[25] Z. Zhang, H. Wang, H. Wang, C. Wu, M. Li, L. Li, Fabrication and evaluation of molecularly imprinted magnetic nanoparticles for selective recognition and magnetic separation of lysozyme in human urine, Analyst 143 (2018) 5849–5856. doi:https://doi.org/10.1039/C8AN01746H.

[26] J.-P. Fan, J.-X. Yu, X.-M. Yang, X.-H. Zhang, T.-T. Yuan, H.-L. Peng, Preparation, characterization, and application of multiple stimuli-responsive rattle-type magnetic hollow molecular imprinted poly (ionic liquids) nanospheres (Fe_3O_4@void@pilmip) for specific recognition of protein, Chemical Engineering Journal 337 (2018) 722 – 732. doi:https://doi.org/10.1016/j.cej.2017.12.159.

[27] H. Zhu, H. Yao, K. Xia, J. Liu, X. Yin, W. Zhang, J. Pan, Magnetic nanoparticles combining teamed boronate affinity and surface imprinting for efficient selective recognition of glycoproteins under physiological ph, Chemical Engineering Journal 346 (2018) 317 – 328. doi:https://doi.org/10.1016/j.cej.2018.03.170.

[28] T. Sulistyaningsih, S. J. Santosa, D. Siswanta, B. Rusdiarso, Synthesis and characterization of magnetites obtained from mechanically and sonochemically assissted co-precipitation and reverse co-precipitation methods, Int J Mater, Mech Manuf 5 (1) (2017) 16–9. doi:https://doi.org/10.18178/ijmmm.2017.5.1.280.

[29] V. Sagar, V. S. R. Atluri, A. Tomitaka, P. Shah, A. Nagasetti, S. Pilakka-Kanthikeel, N. El-Hage, A. McGoron, Y. Takemura, M. Nair, Coupling of transient near infrared photonic with magnetic nanoparticle for potential dissipation-free biomedical application in brain, Scientific reports 6 (2016) 29792. doi:https://doi.org/10.1038/srep29792.

[30] A. Le-Bail, H. Duroy, J. Fourquet, Ab-initio structure determination of lisbwo6 by x-ray powder diffraction, Materials Research Bulletin 23 (3) (1988) 447 – 452. doi:https://doi.org/10.1016/0025-5408(88)90019-0.

[31] J. Rodríquez-Carvajal, T. Roisnel, Line broadening analysis using fullprof*: Determination of microstructural properties, in: European Powder Diffraction EPDIC 8, Vol. 443 of Materials Science Forum, Trans Tech Publications Ltd, 2004, pp. 123–126. doi:https://doi.org/10.4028/www.scientific.net/MSF.443-444.123.

[32] M. Zambrzycki, A. Fraczek-Szczypta, Conductive hybrid polymer composites based on recycled carbon fibres and carbon nanofillers, Journal of materials science 53 (10) (2018) 7403–7416. doi:https://doi.org/10.1007/s10853-018-2062-5.

[33] S. N. A. Keivani, M. Naderi, G. Amoabediny, Superparamagnetic plasmonic nanocomposites: Synthesis and characterization studies, Chemical Engineering Journal 264 (2015) 66 – 76. doi:https://doi.org/10.1016/j.cej.2014.11.059.

[34] S. F. Tanner, H. Chanzy, M. Vincendon, J. C. Roux, F. Gaill, High-resolution solid-state carbon-13 nuclear magnetic resonance study of chitin, Macromolecules 23 (15) (1990) 3576–3583. doi:https://doi.org/10.1021/ma00217a008.

[35] G. Mariotti, L. Vannozzi, Fabrication, characterization, and properties of poly (ethylene-co-vinyl acetate) composite thin films doped with piezoelectric nanofillers, Nanomaterials 9 (8) (2019) 1182. doi:https://doi.org/10.3390/nano9081182.

[36] D. Cangialosi, V. M. Boucher, A. Alegría, J. Colmenero, Physical aging in polymers and polymer nanocomposites: recent results and open questions, Soft Matter 9 (36) (2013) 8619–8630. doi:https://doi.org/10.1039/C3SM51077H.

[37] Z. Tian, S. Wang, X. Hu, Z. Zhang, L. Liang, Crystalline reduction, surface area enlargement and pore generation of chitin by instant catapult steam explosion, Carbohydrate Polymers 200 (2018) 255 – 261. doi:https://doi.org/10.1016/j.carbpol.2018.07.075.

[38] V. Daboin, S. Briceño, J. Suárez, G. Gonzalez, Effect of the dispersing agent on the structural and magnetic properties of $CoFe_2O_4/SiO_2$ nanocomposites, Journal of Magnetism and Magnetic Materials 451 (2018) 502–506. doi:https://doi.org/10.1016/j.jmmm.2017.08.043.

[39] G. F. Goya, T. Berquo, F. Fonseca, M. Morales, Static and dynamic magnetic properties of spherical magnetite nanoparticles, Journal of applied physics 94 (5) (2003) 3520–3528. doi:https://doi.org/10.1063/1.1599959.

[40] B. Juarez-de la Rosa, J. May-Crespo, P. Quintana-Owen, W. Gónzalez-Gómez, J. Yañez-Limón, J. Alvarado-Gil, Thermal analysis and structural characterization of chitinous exoskeleton from two marine invertebrates, Thermochimica Acta 610 (2015) 16–22. doi:https://doi.org/10.1016/j.tca.2015.04.015.

[41] J.-Y. Lee, Y. Liao, R. Nagahata, S. Horiuchi, Effect of metal nanoparticles on thermal stabilization of polymer/metal nanocomposites prepared by a one-step dry process, Polymer 47 (23) (2006) 7970–7979. doi:https://doi.org/10.1016/j.polymer.2006.09.034.

[42] F. Wolman, M. Baieli, N. Urtasun, A. Navarro del Canizo, M. Miranda, O. Cascone, Strategies to recover and purify lysozyme from egg white, Lysozymes: Sources, Functions and Role in Disease. New York: Nova Science Publishers, Inc (2013) 241–250.

[43] J. Chen, Y. Lin, L. Jia, Preparation of anionic polyelectrolyte modified magnetic nanoparticles for rapid and efficient separation of lysozyme from egg white, Journal of Chromatography A 1388 (2015) 43–51. doi:https://doi.org/10.1016/j.chroma.2015.02.032.

[44] J. Sun, Y. Su, S. Rao, Y. Yang, Separation of lysozyme using superparamagnetic carboxymethyl chitosan nanoparticles, Journal of Chromatography B 879 (23) (2011) 2194–2200. doi:https://doi.org/10.1016/j.jchromb.2011.05.052.

[45] J. E. Basconi, G. Carta, M. R. Shirts, Effects of protein properties on adsorption and transport in polymer-grafted ion exchangers: A multiscale modeling study, AIChE Journal 63 (10) (2017) 4564–4575. doi:https://doi.org/10.1002/aic.15798.

[46] T. Gu, K.-H. Hsu, M.-J. Syu, Scale-up of affinity chromatography for purification of enzymes and other proteins, Enzyme and microbial technology 33 (4) (2003) 430–437. doi:https://doi.org/10.1016/S0141-0229(03)00141-8.

[47] I. Šafařík, M. Šafarařík ová, Batch isolation of hen egg white lysozyme with magnetic chitin, Journal of Biochemical and Biophysical methods 27 (4) (1993) 327–330. doi:ttps://doi.org/10.1016/0165-022X(93)90013-E.

[48] I. Šafařík, Magnetic biospecific affinity adsorbents for lysozyme isolation, Biotechnology Techniques 5 (2) (1991) 111–114. doi:https://doi.org/10.1007/BF00159981.

[49] Ö. Acet, A. Menteş, M. Odabaşı, Assessment of a new dual effective combo polymer structure for separation of lysozyme from hen egg white, Polymer Bulletin (2019) 1–17doi:https://doi.org/10.1007/s00289-019-02959-w.